Intercontinental comparison of optical atomic clocks through very long baseline interferometry

26 April 2024

Intercontinental comparison of optical atomic clocks via very long baseline interferometry

Marco Pizzocaro[1*], Mamoru Sekido[2*], Kazuhiro Takefuji[2,†]
Hideki Ujihara[2], Hidekazu Hachisu[3], Nils Nemitz[3],
Masanori Tsutsumi[3], Tetsuro Kondo[2,4], Eiji Kawai[2],
Ryuichi Ichikawa[3], Kunitaka Namba[3], Yoshihiro Okamoto[3],
Rumi Takahashi[3], Junichi Komuro[3], Cecilia Clivati[1],
Filippo Bregolin[1], Piero Barbieri[1], Alberto Mura[1],
Elena Cantoni[1], Giancarlo Cerretto[1], Filippo Levi[1],
Giuseppe Maccaferri[5], Mauro Roma[5], Claudio Bortolotti[5],
Monia Negusini[5], Roberto Ricci[1,5], Giampaolo Zacchiroli[5],
Juri Roda[5], Julia Leute[6,7], Gérard Petit[6], Federico Perini[5],
Davide Calonico[1], Tetsuya Ido[3]

[1]Istituto Nazionale di Ricerca Metrologica (INRIM), Torino, Italy.
[2]National Institute of Information and Communications Technology (NICT), Kashima, Japan.
[3]National Institute of Information and Communications Technology (NICT), Koganei, Tokyo, Japan.
[4]Chinese Academy of Sciences, Shanghai Astronomical Observatory, China.
[5]Istituto Nazionale di Astrofisica (INAF), Istituto di Radioastronomia (IRA), Bologna, Italy.
[6]Bureau International des Poids et Mesures (BIPM), Sèvres, France.
[7]LNE-SYRTE, Observatoire de Paris, Université PSL, CNRS, Sorbonne Université, Paris, France.
*Corresponding authors. Email: m.pizzocaro@inrim.it, sekido@nict.go.jp
†Present address: Japan Aerospace Exploration Agency (JAXA), Nagano, Japan.

ACCEPTED MANUSCRIPT

published as:
Pizzocaro, M., Sekido, M., Takefuji, K. et al.
Intercontinental comparison of optical atomic clocks through very long baseline interferometry.
Nat. Phys. (2020).
https://doi.org/10.1038/s41567-020-01038-6
https://www.nature.com/articles/s41567-020-01038-6

The comparison of distant atomic clocks is foundational to international timekeeping, global positioning and tests of fundamental physics. Optical fibre links allow the best optical clocks to be compared without degradation over distances up to thousands of kilometres, but intercontinental comparisons remain limited by the performance of satellite transfer techniques. Here we show that very long baseline interferometry (VLBI), although originally developed for radio astronomy and geodesy, can overcome this limit and compare remote clocks through observing extragalactic radio sources. We developed dedicated transportable VLBI stations that use broadband detection and we compared two optical clocks in Italy and Japan separated by 9000 km. This system demonstrates performance beyond satellite techniques and can pave the way for future long-term stable international clock comparisons.

Atomic clocks based on optical transitions can reach fractional uncertainties at the 10^{-18} level[1–3] surpassing by two orders of magnitude the microwave clocks[4] that realize the definition of the second in the International System of Units (SI) and are the basis of international timekeeping[5]. Given the rapid progress of optical clocks, a redefinition of the SI second as the unit of time is anticipated[6]. The remote comparison of different clocks worldwide is fundamental to check their consistency in view of such a redefinition. It is also attractive for challenging experiments such as tests of special and general relativity[7–9], laboratory searches for the variations of fundamental constants[10,11], and measurements of Earth's gravitational potential[12–14]. Future applications of clock comparisons include the search for dark matter[15], the establishment of quantum networks for secure communications and timing[16] and gravitational wave detection[17]. Optical fibre links have been shown to allow comparisons at the full accuracy of the clocks up to thousands of kilometres[18]. However, they have not reached a transoceanic scale[19] and therefore intercontinental comparisons are only possible by microwave satellite transfer techniques[20]. Among these are two-way time-and-frequency transfer, which makes use of geostationary telecommunication satellites[21,22], or precise point positioning[23], which relies on the constellation of the Global Positioning System (GPS). These techniques achieve a typical uncertainty at the level of 10^{-15} at 1 d of averaging time that limits the comparison of optical clocks.

Very long baseline interferometry (VLBI) is a technique developed for radio astronomy and geodesy[24,25] based on the simultaneous observation of remote radio sources with distant antennas, each referenced to a local atomic clock. Since its early development, VLBI has been considered for synchronization of the reference clocks[26,27] but it has never been exploited for this task due to the convenient use of satellites. Recently, VLBI has been proposed to improve intercontinental frequency links[28] and has been suggested for the comparison of optical clocks[29]. Here we demonstrate a VLBI system dedicated to frequency transfer with broadband detection that allows for better performance than satellite techniques.

VLBI cross-correlates the signals arriving from astronomical radio sources to different antenna locations. The geometrical delay between two stations $\tau_{\mathrm{geom}} = \boldsymbol{B} \cdot \boldsymbol{S}/c$ depends on the baseline between the antennas $\boldsymbol{B}$ and the unit vector to the radio source $\boldsymbol{S}$, with c the speed of light. The observed value τ_{obs} differs from the geometrical delay because of the timing offset between the reference clocks $\mathit{\Delta}\tau_{\mathrm{clock}}$ and it is additionally affected by the station-to-station difference in excess delays introduced by atmosphere $\mathit{\Delta}\tau_{\mathrm{atm}}$, ionosphere $\mathit{\Delta}\tau_{\mathrm{ion}}$, instruments such as antennas, cables, and receivers $\mathit{\Delta}\tau_{\mathrm{instr}}$, and ultimately the radio source structure $\mathit{\Delta}\tau_{\mathrm{source}}$:

$$\tau_{\mathrm{obs}} = \tau_{\mathrm{geom}} + \mathit{\Delta}\tau_{\mathrm{atm}} + \mathit{\Delta}\tau_{\mathrm{ion}} + \mathit{\Delta}\tau_{\mathrm{instr}} + \mathit{\Delta}\tau_{\mathrm{source}} + \mathit{\Delta}\tau_{\mathrm{clock}}. \tag{1}$$

The different components of the delay can be either modelled, estimated from the observations, or obtained as a result of separate measurements depending on the application. Radio astronomy is interested in studying radio source structure while geodetic VLBI seeks to minimize its effects by selecting point-like sources in the interest of determining precise station coordinates and monitoring variations in Earth rotation. The International Celestial Reference Frame (ICRF) as adopted by the International Astronomical Union (IAU)[30] provides a suitable list of extragalactic radio sources that are regarded as fiducial points in the sky. Calibration of excess atmospheric delay is made by an atmospheric model based on weather data[31], which is represented by a zenith delay and a mapping function for observations at different elevation angles generated by ray tracing techniques. The ionospheric delay has a characteristic frequency dependence that allows its calibration directly from observation data. VLBI measurements typically use local active hydrogen masers as stable frequency references. When all effects are considered, it is possible for VLBI measurements to provide the frequency difference between the hydrogen masers and thus compare any clocks or timescales locally linked to them.

We designed and built two transportable VLBI stations with 2.4 m diameter Cassegrain antennas. These stations implement the concept of broadband VLBI observation proposed as VLBI Global Observing System (VGOS) by the International VLBI Service for Geodesy and Astrometry (IVS)[32] to reach 1 mm position accuracy in geodetic measurements. Whereas standard geodetic VLBI only makes observations in narrow frequency ranges in the S band (2.2 GHz–2.4 GHz) and X band (8.2 GHz–8.95 GHz)[25], the stations in this work can access frequencies from 3 GHz to 14 GHz. Our receivers first acquire data with a sampling rate of 16 GHz and then digital filters extract the signals in four 1 GHz wide channels spread over the wide frequency range. Integration of the four channels determines precise group delays using the bandwidth synthesis technique[33]. We employ a 2048 MHz sampling rate in each channel, where conventional VLBI uses 32 MHz or below, enhancing the signal-to-noise ratio by a factor of 8. Improved signal-to-noise ratio allows for smaller overall dish area of the antennas. By itself, the enhanced detection bandwidth is not sufficient for measurements over an intercontinental baseline with easily transportable dish sizes. This is overcome by including the 34 m radio antenna operated by NICT in Kashima (Japan) in a joint node-hub style observation: the delay observable between the transportable stations (nodes) can be calculated as the difference of the two delays with the large antenna (hub) after applying a small correction factor (see Methods). This measurement benefits from the improvement of the equivalent dish area, which scales as the geometrical mean, without the penalties specific to large antennas since the delay variations due to gravitational distortion of the large dish or temperature dependence in long cables are largely reduced as a common-mode noise.

Here, one node was installed at NICT headquarters in Koganei (Japan) while the other was transported to the Radio Astronomical Observatory operated by INAF in Medicina (Italy), forming an intercontinental baseline of 8700 km (see Fig. 1). Observation data at Medicina and Koganei were stored on hard-disk drives at each station and transferred over high-speed Internet networks to the correlation center in Kashima for analysis. Ten frequency measurements via VLBI were performed between October 2018 and February 2019 from which we calculated the frequency difference between the reference clocks at the two stations: the local hydrogen masers in Medicina and in Koganei. Each session lasted from 28 h to 36 h and included at least 400 scans observing between 16 and 25 radio sources in the ICRF list. A least-squares fit of each run was used to calculate the observed delay with typical residuals of 30 ps and a formal uncertainty in the frequency comparison as low as 1.5×10^{-16} for a single run (see Extended Data Table 1). At this level of uncertainty, accurate modelling of atmospheric delays is a crucial part of the analysis (see Methods).

We used this VLBI frequency link to compare two optical clocks: the ytterbium-171 optical lattice clock[34] IT-Yb1 at INRIM in Torino (Italy) and the strontium-87 optical lattice clock[35,36] NICT-Sr1 in Koganei. Both optical clocks are realizations of the unit of time, formally recognized within the Metre Convention. This is possible because the frequency values of ytterbium and strontium clock transitions are recommended as secondary representations of the second in the list of standard reference frequency values[6,37] of the International Committee for Weights and Measures (CIPM) with frequencies $f(\mathrm{Yb}) \approx 518\,\mathrm{THz}$ and $f(\mathrm{Sr}) \approx 429\,\mathrm{THz}$ and with relative uncertainties of 5×10^{-16} and 4×10^{-16} respectively. Therefore, the frequency ratio between IT-Yb1 and NICT-Sr1 can be compared to the officially recommended values in addition to previous measurements[13,22,38,39].

The frequency comparison between IT-Yb1 and NICT-Sr1 followed the chain shown in Fig. 1. In Torino, the ytterbium clock was compared to a local hydrogen maser using an optical frequency comb[40], which allows precise optical-to-microwave frequency comparisons. The comb in Torino also measured a narrow-linewidth laser at telecommunication wavelengths that was sent on a compensated optical fibre link[41] of 535 km to the Radio Observatory in Medicina. Here, another optical frequency comb compared the laser fibre-delivered from Torino with the hydrogen maser referencing the VLBI station. In Koganei, a third optical frequency comb was used for the comparison of the strontium clock with local hydrogen masers, including the maser used as reference for the VLBI station.

Since the optical clocks, optical link and VLBI link operated intermittently throughout this campaign we extrapolate the hydrogen maser frequencies[42,43] to calculate a frequency ratio for each VLBI run. Figure 2a shows the results of the ratio measurements, with uncertainties evaluated for each step of the frequency chain including the extrapolations (see Methods). The weighted mean for the campaign is the frequency ratio $R = f(\mathrm{Yb})/f(\mathrm{Sr}) = 1.207\,507\,039\,343\,338\,05(34)$ measured via VLBI. This corresponds to a fractional deviation from the ratio R_0 of the recommended frequencies for ytterbium and strontium of $y(\mathrm{Yb/Sr}) = R/R_0 - 1 = 2.5(2.8) \times 10^{-16}$ in agreement with previous measurements (see Fig. 2b). Over the course of the campaign, the overall VLBI measurement contributes a one-standard-deviation uncertainty of only 9×10^{-17} for a total measurement time of 300 h. The optical link, conversion to microwave signals, maser frequency extrapolation and systematic effects in the optical clocks contribute to the overall uncertainty of 2.8×10^{-16} as reported in Table 1. The gravitational redshift induced by the different gravitational potential at the position of the optical clocks[34,35] has been accounted for in the clock systematic shifts, bringing a relative correction of $-1.765(2) \times 10^{-14}$ to the frequency ratio.

To confirm the results, we established an independent frequency link using GPS satellites between receivers at INRIM and at NICT (see Fig. 1). To achieve low uncertainty on this link, we calculated a precise point positioning solution with integer ambiguity resolution (IPPP)[44]. For this baseline, IPPP has an uncertainty of 9×10^{-16} at 1 d of averaging time. The comparison of the ytterbium and strontium optical clocks using the IPPP solution over the same time intervals as the VLBI runs is also shown in Fig. 2a. The weighted mean of the frequency deviation of the ratio is $y(\mathrm{Yb/Sr}) = -3.2(4.0) \times 10^{-16}$ measured via IPPP. As shown in Table 1, the GPS link contributes an overall uncertainty for the campaign of 2.6×10^{-16}. We can also compare the VLBI and IPPP results directly, closing the loop via the optical link, and the weighted mean of the differences for the entire

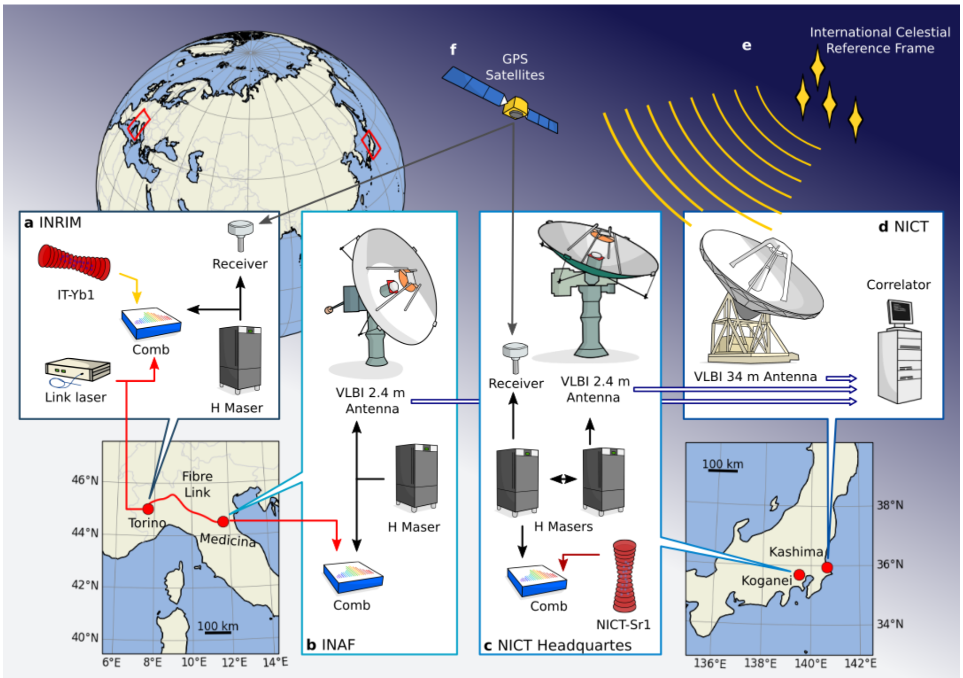

Figure 1: Schematic representation of the frequency link between the ytterbium and strontium optical clocks via VLBI and satellite transfer. a, In Torino, IT-Yb1 at INRIM is compared with the local hydrogen maser and the link laser using an optical frequency comb. The link laser is sent over compensated fibre link to Medicina. **b,** In Medicina, at INAF Radio Observatory, the incoming link laser is compared with the local hydrogen maser using another optical frequency comb. The first transportable broadband VLBI station is setup in Medicina and referenced to this maser. **c,** In Koganei, the second VLBI station at NICT headquarters is referenced to a local hydrogen maser. NICT-Sr1 is compared to the local hydrogen maser using a third optical frequency comb, ending the chain. **d,** The 34 m diameter radio telescope maintained by NICT in Kashima assisted in the node-hub style observations, increasing the signal-to-noise ratio. The observation data in Medicina and Koganei were transferred to the correlation center in Kashima over high-speed internet networks (blue arrows). The cross-correlation between the antennas and the following geodetic analysis allows to measure the reference clock difference. **e,** The VLBI link is established by observing several radio sources in the International Celestial Reference Frame. **f,** A satellite frequency link with GPS satellites is established between the receivers in Torino and Koganei.

Table 1: Uncertainty budgets for the ratio and closure measurements. The listed uncertainties are calculated for the weighted average of the points in Figure 2a and the weighted average of their difference. The VLBI and IPPP uncertainties are the statistical contribution for the frequency transfer. The clock contributions consist of the systematic uncertainties of both clocks, including the gravitational redshift. The extrapolation uncertainty is a statistical uncertainty due to the intermittent operations of the optical clocks and the optical link. The uncertainty for the combs arises from their accuracy and from the instability in the microwave to optical conversions. The optical link contribution is negligible for the present measurement. All uncertainties correspond to one standard deviation.

Yb/Sr ratio via VLBI		Yb/Sr ratio via IPPP		Closure	
Contribution	Uncer. ($\times 10^{-16}$)	Contribution	Uncer. ($\times 10^{-16}$)	Contribution	Uncer. ($\times 10^{-16}$)
VLBI	0.9	IPPP	2.6	VLBI	0.7
Clocks	0.9	Clocks	0.9	IPPP	2.3
Combs (microwave/optical)	1.1	Combs (microwave/optical)	1.1	Combs (microwave/optical)	1.1
Extrapolation	2.2	Extrapolation	2.6	Extrapolation	1.9
Optical link	<0.1			Optical link	<0.1
Total	2.8	Total	4.0	Total	3.2

campaign is $y(\text{VLBI-IPPP}) = 3.5(3.2) \times 10^{-16}$.

By leveraging broadband observations, our VLBI system surpasses the best satellite techniques and what is possible with traditional geodetic VLBI, resulting in a typical formal uncertainty of 2×10^{-16} at 10^5 s of averaging time. It has the potential to reach uncertainty in the low 10^{-17} region at 10 d of averaging time provided variations in instrumentation delay are minimized, radio sources are carefully selected to minimize structure effects, and the atmosphere is accurately modelled. Although VLBI still requires optical to microwave conversions, this is an attractive technique for optical clocks comparisons. With increased operational duty times of the optical clocks and improved characterization of the combs [45] and of the frequency chains, it will allow for link uncertainties that approach the systematic uncertainties of optical clocks for manageable measurement times.

Our measurements show agreement between the VLBI link, the optical clocks and the GPS link at the low 10^{-16} level. There is still some uncertainty on the optimal treatment for the calibration of the tropospheric delay in a VLBI experiment with a long single baseline and further investigation should clarify the correlation with the estimated clock frequency. We have estimated that thermal sensitivity of the cables and of the antennas contributed an uncertainty less than 1×10^{-17}. The microwave signal acquired by the antenna is transferred to the data acquisition system by amplitude

a

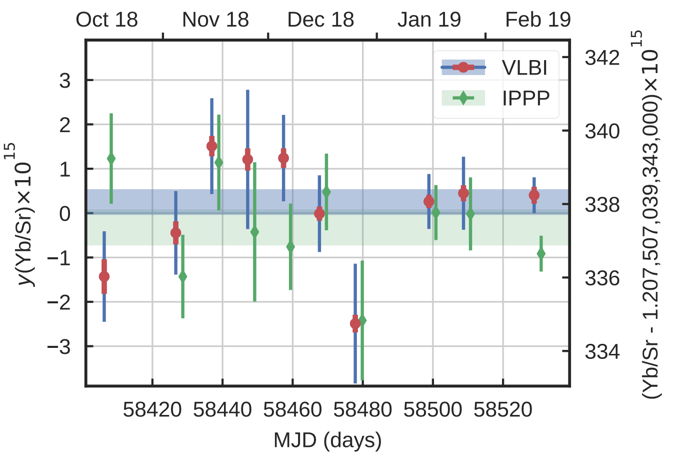

b

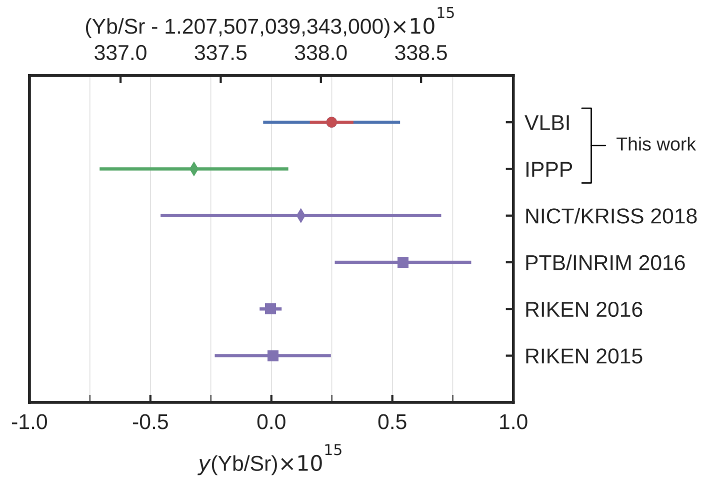

Figure 2: Comparison of Yb/Sr frequency ratio measurements. a, Ratio measurements for each VLBI run at a given Modified Julian Date (MJD) measured via VLBI or IPPP. Red bars represent the statistical uncertainty of the VLBI link only, while blue bars represent the total uncertainty for the VLBI comparisons (including optical clocks, optical combs, and extrapolations). Blue shaded region is the weighted mean of the VLBI comparison with its total uncertainty. Green points represent the IPPP comparisons with their total uncertainty. Green shaded region is the weighted mean of the IPPP comparison with its total uncertainty. Horizontal offset between the two dataset is for clarity. **b,** Optical frequency ratio $f(\mathrm{Yb})/f(\mathrm{Sr})$ as measured in this work (red/blue and green points as in a) or in previous measurements where purple squares represent local measurements at RIKEN[38,39] and by PTB and INRIM[13] and the purple diamond denotes a remote measurement performed by NICT and KRISS[22]. All uncertainties correspond to one standard deviation.

modulation of an infrared laser over fibre. In Medicina, a 600 m long underground fibre is used, with frequency shifts less than 8×10^{-17} in a day. In our experiment, we observed excess delay residuals for 3 of the 35 observed sources caused by the source structure effect[46,47]. The increased residuals are accounted for in the fit procedure but a careful selection of radio sources will help to avoid systematic effects in future clock comparisons. On the other hand, transportable broadband antennas may play a significant role to increase the density and extend the baselines in large networks of antennas, with the aim to improve investigations of source with structure.

The endpoint VLBI stations are transportable and can be deployed close to time-and-frequency laboratories just like traditional satellite antennas, supported by the node-hub topology. They can be operated without the need for a radio transmission license and, with a higher data transmission capability, they may provide a continuous link instead of the separate sessions used in our measurements. Where laboratories lack the facilities or sky coverage to house a VLBI station, they can be connected by local optical fibre links, as demonstrated here. It is envisioned that optical clock comparisons will increasingly rely on local area fibre networks connected by non-fibre intercontinental links, with application in precision timing, searches for new physics and clock-based geodesy[48]. Proposals for improved intercontinental links includes IPPP[44], carrier-phase two way frequency transfer[49], and the use of transportable optical clocks[13] or dedicated orbital systems such as the planned Atomic Clock Ensemble in Space (ACES) mission[50]. Our experiment realizes such a hybrid network with a high performance VLBI link, useful for primary metrology and fundamental physics.

Methods

Broadband VLBI observation system

In VLBI observations, the standard deviation of the observed group delay is given by

$$\sigma_\tau = \frac{1}{2\pi R_{\mathrm{sn}} \mathit{\Delta} f_{\mathrm{rms}}}, \tag{2}$$

where $\mathit{\Delta} f_{\mathrm{rms}}$ is the root mean square deviation of the observation frequencies f_i while the signal to noise ratio is given by

$$R_{\mathrm{sn}} = \eta \sqrt{\frac{A_1 A_2 B t}{T_1 T_2}} \frac{S}{2k_{\mathrm{B}}}, \tag{3}$$

where A_j are the effective areas of the two antennas, T_j the system noise temperatures, B is the observation bandwidth, t is the integration time, S is correlated flux density of the radio source, k_{B} is Boltzmann's constant and η is a digital processing loss factor[51]. Delay observations can thus be improved by increasing the spread of observation frequency Δf_{rms} and the bandwidth B of the observations.

The VLBI observation system used in this experiment, GALA-V[52], implements data acquisition according to the VGOS standard, which aims at making broadband observations spread over the frequency range of 2 GHz–14 GHz. NICT developed a unique broadband feed[53] named NINJA, with constant narrow beam size for wide frequency range, which enables broadband observation with existing Cassegrain antennas. The NINJA broadband feeds were installed in the two transportable 2.4 m diameter antennas and the Kashima 34 m diameter antenna. The transportable antennas acquire a single linear (V) polarization signal. To avoid a loss of correlation from the different polarizations observed by distant stations due to parallactic angle, the hub station in Kashima acquires both (V and H) polarizations. The VH and VV data sets are then processed coherently.

The data-acquisition we adopted uses four channels with $B = 1024$ MHz bandwidth at frequencies $f_1 = 6.0$ GHz, $f_2 = 8.5$ GHz, $f_3 = 10.4$ GHz and $f_4 = 13.3$ GHz. This system is simpler than the prototype VGOS proof-of-concept implementation[32], which acquires data on more than one hundred channels with 32 MHz frequency bandwidth. Our array of selected frequencies provides a sharply peaked delay resolution function (see Extended Data Fig. 1), and the large bandwidth of each channel allows the unambiguous determination of the absolute group delay using the technique of bandwidth synthesis[33,54]. Since the group delay has a linear phase slope over frequency, a stable phase relation between adjacent channels is essential and it is assured by a fully digital signal processing. We employ high-speed radio frequency direct sampling[55] to digitize the signal without any analog frequency conversions: the received signal is amplified, and then first converted to digital data with a 16 384 MHz sampling rate via the high-speed sampler K6/GALAS[52]. A digital filter implemented on a field programmable gate array (FPGA) extracts the four signal channels with 1-bit sampling at 2048 megasamples per second for each polarization. Observation data is stored on hard-disk drives at each station, and then transferred to the station at Kashima over high-speed research networks for correlation processing.

Node-hub style VLBI observations

Transportable VLBI systems have previously been investigated for geodetic VLBI[56,57], although their sensitivity is limited by the physical size of the collecting area.

Our broadband observation system allows for smaller antennas by increasing the observation bandwidth (Eq. 3). Yet, even in this case, the transportable antenna pair does not have enough sensitivity for the reduced correlated flux density on an intercontinental baseline. This is overcome by combining the small transportable antennas (nodes) with a high sensitivity antenna (hub). The baseline between the smaller stations is then deduced by a closure delay relation[58]. For two node stations A and B and a hub station R making an observation of a point-like radio source (see Extended Data Fig. 2) the time delay differences at time t for the arrival of an identical wave are related by the linear combination

$$\tau_{\mathrm{AB}}(t) = \tau_{\mathrm{RB}}(t) - \tau_{\mathrm{RA}}(t) - \dot{\tau}_{\mathrm{AB}}(t) \cdot \tau_{\mathrm{RA}}(t). \quad (4)$$

Higher order terms in this relation are negligible for any terrestrial baselines when the radio source structure effect is negligible. The uncertainty of the delay τ_{AB} calculated in this way is still dominated by the contributions of instruments, atmosphere and source structure at the nodes as if the delay had been measured directly. In obtaining the delay observable of the AB baseline, the delay properties of station R such as atmospheric delay, cable length change, and gravitational deformation of the dish are canceled out. In our case, with both the hub and a transportable station separated by only 110 km, Eq. 4 is still valid even in the presence of radio source structure, because the short baseline is insensitive while only the effect on the baseline AB is observed.

VLBI signal processing and analysis

The data reduction procedure for the VLBI observation consists of three steps for each of the node-hub baselines: first, the individual VH and VV polarization pairs for each frequency band are cross-correlated and time integration is made using the software correlator GICO3[59] running on a cluster of computers. Second, synthetic cross-correlation data is generated by combining the VH and VV data such that correlation amplitudes are maximized for each scan and frequency band. Third, wideband bandwidth synthesis[33] is applied to derive wideband group delay observables. Here we account for phase shifts of the propagating electromagnetic signal introduced by the ionospheric dispersive medium in the form of $\phi = A \cdot \delta_{\mathrm{TEC}}/f$, where δ_{TEC} is the difference of total electron content (TEC) in the line of sight from each observation station, f is the radio frequency of the observations and A is a constant given by $e^2/(4\pi c \varepsilon_0 m_e)$, with ε_0 the vacuum electric permittivity and m_e the mass of the electron. The wideband bandwidth synthesis procedure calibrates ionospheric delay by simultaneously estimating δ_{TEC} and broadband group delay. Group delay data for all scans and baselines is stored in a Mark3 VLBI database. The virtual delays on the baseline between transportable antennas is analysed by a least-square fit using the Calc/Solve software[60]. The parameters of the fit were the coordinates of one station, the atmospheric delay parameters for both stations as piecewise linear functions with 60 minutes intervals and a single clock offset and clock rate.

The observed radio sources were selected from the recently proposed ICRF3 list[61], which provides accurately known coordinates that predict the geometrical delays. The a-priori delay calculation includes relativistic coordinate transformation from the solar barycentric frame to a geocentric frame comoving with the Earth, accounting also for the gravitational time delay[62]. The excess path caused by dry atmosphere can be accurately predicted from air pressure on the ground, height, and latitude of the station[63]. However, the distribution of water vapour is hard to predict from ground weather data, and the anisotropy of the atmosphere is difficult to estimate directly from the VLBI data because the east-west long baseline results in a limited sky coverage. Thus, we use the Vienna Mapping Functions 3 (VMF3)[64] for a priori delay calibration. The VMF3 are computed by ray tracing within a numerical weather model of the European Centre for Medium-Range Weather Forecasts (ECMWF). They include dry and wet components, as well as gradients, in the model data. Their data is publicly available and regularly computed for most space geodetic observation sites including Kashima, Koganei, and Medicina. Residuals atmospheric contributions were estimated in the least-squares analysis of VLBI data.

Uncertainty of the optical clocks, optical link and combs

The operation of IT-Yb1 and NICT-Sr1 is similar and presented in detail in ref.[34,35,42,65]. In both systems, an ultrastable clock laser is stabilized to the clock transition of atoms cooled to microkelvin temperatures and trapped in an optical lattice at the magic wavelength[66], 759 nm for ytterbium and 813 nm for strontium. Frequency combs measure the clock laser relative to the local hydrogen masers.

For this campaign, the systematic frequency shifts of the clocks have been characterized with an uncertainty of 3.1×10^{-17} for IT-Yb1 and 8×10^{-17} for NICT-Sr1. The lattice light shift, density shift and static Stark shift are evaluated by interleaving measurements in different conditions. The blackbody radiation shift is calculated from the temperature of the physics package of each clock using known atomic parameters[67–69], where the uncertainty is dominated by temperature inhomogeneity. We calculated from known atomic coefficients the lattice hyperpolarizability and multipolar shift[70–72], the quadratic Zeeman shift[1,72–76], the background gas shift[1,77] and the probe light shift[1,78].

At both laboratories, we determined the gravitational redshift with respect to the conventionally adopted gravity potential[79] $W_0 = 62\,636\,856.0\,\mathrm{m^2s^{-2}}$. At INRIM, the redshift is calculated from a gravitational potential difference measured with a global navigation satellite system/geoid approach from the geoid model of Europe EGG2015[80,81], with an uncertainty of 3×10^{-18} corresponding to about 3 cm in height. At NICT, the redshift is calculated from the geoid model of Japan GSIGEO2011[82] with an uncertainty of 2×10^{-17}, which includes oscillations from tidal effects whose 10-day mean is less than 15 cm in height.

The operation of the combs in Torino and Medicina and of the connecting optical link were monitored by redundantly tracking beatnotes to detect and remove cycle slips in the phase-locked loops. For this task, acquisition in Torino and Medicina was synchronized using the Network Time Protocol at better than 100 ms. The average number of cycle slips during the uptime was less than one per hour. The fibre-delivered laser is loosely phase locked to the hydrogen maser in Torino using the comb to avoid frequency drifts. In these conditions, the optical link contributes less than 1×10^{-18} after 1000 s of averaging time[41,83].

For this measurement, the optical-to-microwave comparison at the combs in Torino, Medicina and Koganei has been evaluated at an uncertainty of 8×10^{-17} each, while optical-to-optical comparisons are better characterized[84] at less than 1×10^{-18}. We also conservatively estimated that each optical-to-microwave comparison at the comb introduces phase noise with a corresponding instability of 2×10^{-14} at 1 s of averaging time. The instabilities of the optical clocks are negligible compared to those of the maser frequency measurements, at about 2×10^{-15} at 1 s for the ytterbium clock and 7×10^{-15} at 1 s for the strontium clock.

Uncertainty in the frequency chain

The calculation of the frequency chain for the VLBI measurement of optical clocks follows the measurement model:

$$\frac{f(\mathrm{Yb})}{f(\mathrm{Sr})} = \frac{f(\mathrm{Yb})}{f(\mathrm{H_T})} \frac{f(\mathrm{H_T})}{f(\mathrm{H_M})} \frac{f(\mathrm{H_M})}{f(\mathrm{H_K})} \frac{f(\mathrm{H_K})}{f(\mathrm{Sr})}, \tag{5}$$

where the $f(\mathrm{Yb})/f(\mathrm{H_T})$ is the frequency ratio between the ytterbium optical clock and the hydrogen maser in Torino measured at the comb, $f(\mathrm{H_T})/f(\mathrm{H_M})$ is the frequency ratio between the masers in Torino and in Medicina measured using the optical fibre link, $f(\mathrm{H_M})/f(\mathrm{H_K})$ is the frequency ratio between the masers in Medicina and in Koganei measured using the VLBI comparison, and $f(\mathrm{H_K})/f(\mathrm{Sr})$ is the frequency ratio between the hydrogen maser in Koganei and the strontium optical clock measured at the comb.

In the data analysis, each ratio r in Eq. (5) is expressed as a fractional deviation $y = r/r_0 - 1$, where r_0 is an arbitrary reference ratio. We chose the reference ratios for the clocks to be consistent with the recommended frequencies of ytterbium and strontium as secondary representations of the second[37], $f_0(\mathrm{Yb}) = 518\,295\,836\,590\,863.6(3)$ Hz and $f_0(\mathrm{Sr}) = 429\,228\,004\,229\,873.00(17)$ Hz. After linearization, the fractional correction of the result $y(f(\mathrm{Yb})/f(\mathrm{Sr}))$ can be calculated as the sum of the fractional corrections of each ratio.

The four frequency ratios in Eq. 5 were not measured simultaneously and need to be extrapolated to common intervals using the hydrogen masers as flywheel oscillators[34,35,85]. After accounting for a linear drift, the dominant contribution to the extrapolation uncertainty is due to the stochastic maser behaviour[42,43,86]. We model the maser noise with a power-law model[87] described by an Hadamard variance $\sigma_{\mathrm{H}}^2 = h_{-2}(\tau/\mathrm{s})^{-2} + h_{-1}(\tau/\mathrm{s})^{-1} + h_0 + h_2(\tau/\mathrm{s})^2$. The coefficients h_j, conventionally identified with white phase noise, white frequency noise, flicker frequency noise and flicker-walk frequency noise respectively, are deduced from comparisons with the optical clocks or within the maser ensembles at INRIM and at NICT (see Extended Data Fig. 3b). The h_2 coefficient provides the best description of the long-term behaviour observed at NICT and it predominantly affects extrapolations over datasets longer than 10 d. There are no significant changes in the overall result if using an alternative set of coefficients that sets $h_2 = 0$ or replaces it with a best-fit h_1 coefficient associated with random-walk noise. We calculated the uncertainty due to dead time by Monte Carlo methods, using an algorithm for the generation of power-law noise[88] and simulating 500 repeated averages over the time periods involved[23,34,35,85]. The numerical calculations agree with analytic results based on the power spectral density of the modelled noise. The drift of each maser was determined from the comparison with the optical clocks and extrapolations were calculated as $d\Delta t$, where d is the measured drift and Δt is the time difference of the barycentres of constituent data for the ratio under investigation. The averaging intervals were carefully selected to only include periods of well-characterized maser behavior. We note that we chose the averaging interval for each step of the chain aiming to minimize the final uncertainty for the ratio via VLBI (see Extended Data Fig. 3a).

The extrapolations have a typical uncertainty of 1×10^{-15} for each VLBI measurement in Fig. 2a. For the last point on MJD 58529, this contribution was reduced to 2.8×10^{-16} by operating all parts of the experiment simultaneously, with residual extrapolation uncertainties only due to downtimes of the optical clocks and of the optical link.

At NICT, the VLBI station and the strontium optical clock were compared to different masers in the available ensemble. Using the continuously operated Japan Standard Time System[89], the conversion between masers can be calculated with a negligible uncertainty of 2×10^{-17} after 10^5 s of measurement time.

The measurement models for the frequency ratio via IPPP and for the closure difference between VLBI, optical link and IPPP employ a similar sequence of calculations but require different extrapolations. The closure calculation does not rely on optical clock data except through the extracted maser drifts.

Averages and statistics of the frequency comparison

In our analysis, we consider the covariance matrix between the various measurements and calculate the weighted averages of Yb/Sr and closure ratios with the Gauss-Markov theorem, or generalized least-squares fit [90,91]. We assume the systematic uncertainties of each clock and each comb as fully correlated over time. In a limited number of cases, the same optical clock data contribute to the ratio evaluation of more than one VLBI run (see Extended Data Fig. 3a) and we account for this correlation.

For our measurements we averaged 190 h of ytterbium clock data, 790 h of the optical link data, 300 h of VLBI sessions and GPS link, and 130 h of strontium clock data. The Birge ratios [91] for the weighted averages over 10 VLBI sessions are $\sqrt{\chi^2/n} = 1.07$ for the VLBI measurement, $\sqrt{\chi^2/n} = 0.90$ for the IPPP measurement, and $\sqrt{\chi^2/n} = 1.32$ for the closure, all with $n = 9$ degrees of freedom.

The Gauss-Markov method is used to establish optimal weights of the data points for each of these measurements. The changing allocation of weights results in a variation of overall uncertainty contributions (e.g., for VLBI and IPPP in Table 1 and for the extrapolation in Extended Data Figure 4) because the weights are calculated from the total uncertainty of each measurement.

Yb/Sr ratio via satellite link

The ratio between the ytterbium clock and the strontium clock with the satellite link reported in the main text only used data coinciding with VLBI runs. We can average the GPS data to calculate a Yb/Sr frequency ratio without this limitation, looking for the best overlap of ytterbium and strontium data in the 130 d of the campaign. We calculated this ratio using both a precise point positioning (PPP) solution and the IPPP solution over the entire campaign (see Extended Data Fig. 4), resulting in frequency deviations $y(\mathrm{Yb/Sr}) = -2.4(4.0) \times 10^{-16}$ using PPP and $y(\mathrm{Yb/Sr}) = -3.1(2.5) \times 10^{-16}$ using IPPP. For these measurements we averaged 180 h of ytterbium clock data, 580 h of satellite transfer and 140 h of strontium clock data. The Birge ratio for the weighted average of these measurements are $\sqrt{\chi^2/n} = 0.53$ for PPP and $\sqrt{\chi^2/n} = 0.29$ for IPPP, both with $n = 9$ degrees of freedom. As expected, IPPP results in a better uncertainty corresponding to a frequency ratio $f(\mathrm{Yb})/f(\mathrm{Sr}) = 1.207\,507\,039\,343\,337\,38(30)$. The significantly longer measurement time ultimately allows this measurement to achieve the same uncertainty as the VLBI result.

Acknowledgements

Development of the broadband feed system was supported by Prof. Kenta Fujisawa of Yamauchi University. We acknowledge Shingo Hasegawa, Yuka Miyauchi of NICT/Kashima Space Technology Center, Fumimaru Nakagawa, Hiroshi Ishijima of NICT/Headquarters, and Takatoshi Ikeda of KDDI Research Laboratory for their contribution to achieve this work. We thank Alice Tabellini of IRA/INAF, Annalisa Dondi and Massimo Alberghini of the Bologna Customs Agency for the management of the temporary importation of the transportable VLBI antenna from Japan to Italy. The broadband feeds were realized through the grant of Joint Development Research on "Development of Broadband receiver system of Kashima 34m" (2013-2015) supported by the Research Coordination Committee, National Astronomical Observatory of Japan (NAOJ), National Institutes of Natural Sciences (NINS). The development of the ytterbium optical clock and of the optical link were supported by the European Metrology Program for Innovation and Research (EMPIR) projects 15SIB03 OC18, 15SIB05 OFTEN, 17IND14 WRITE, 18SIB05 ROCIT; by the Italian Ministry of Education, University and Research (LIFT and Metgesp projects); by the Horizon 2020 Marie Skłodowska-Curie Research and Innovation Staff Exchange (MSCA-RISE) project Q-SENSE (Grant Agreement Number 691156). The EMPIR initiative is co-funded by the European Union's Horizon 2020 research and innovation programme and the EMPIR Participating States. J.L. was supported by the French National Research Agency under the LABEX Cluster of Excellence FIRST-TF (ANR-10-LABX-48-01). Fast data transfer from Italy to Japan for quick turn around of the experiments was realized by support of high research networks JGN, Internet2, TransPAC, APAN, GEANT, and GARR. IPPP results make use of the GINS software developed by the French Space Agency CNES.

Author's contributions

D.C., T.I., and M.S. designed, prepared and coordinated the experiment with contributions from F.P. and F.L. M.S., K.T., H.U., M.T., J.K., and R.I. designed and built the broadband VLBI system. M.S., K.T, H.U., M.T., E.K., K.N., Y.O., and R.T. set up and operated the VLBI stations in Koganei and Kashima. M.S., K.T., M.T., H.U., K.N., Y.O., and R.T. set up and operated the VLBI station in Medicina with support from G.M., M.R., C.B., G.Z., J.R., and F.P. M.P., F.B., and P.B. evaluated and operated the ytterbium clock and the comb in Torino. C.C. and A.M. evaluated and operated the optical fibre link and the combs in Torino and Medicina with support from M.R. and C.B. H.H., N.N., and T.I. evaluated and operated the strontium clock and the comb in Koganei. M.S., K.T., and T.K. carried out the correlation analysis of the VLBI delay data. M.S., M.N., and R.R. carried out the geodetic VLBI analysis. E.C., G.C., R.I., J.L., and G.P. carried out the data analysis of the satellite links. M.P. and M.S. performed the data analysis for the frequency comparisons with contributions from N.N., C.C., J.L. and G.P. M.P. wrote the manuscript with support from M.S., N.N., and C.C. All authors discussed the results and commented on the paper.

Competing interests

The authors declare no competing interests.

Data Availability

The data that support the plots within this paper and other findings of this study are available from the corresponding authors upon reasonable request.

Extended Data Table 1: VLBI sessions used for frequency comparison.

Date	Duration /h	Scans	Sources	Delay res. /ps	Rel. Freq. Unc.
14/10/2018	29	448	22	32	3.9×10^{-16}
04/11/2018	31	463	16	39	2.6×10^{-16}
14/11/2018	29	464	24	24	2.3×10^{-16}
24/11/2018	29	445	23	29	2.5×10^{-16}
04/12/2018	29	471	23	33	2.2×10^{-16}
15/12/2018	29	457	22	26	1.6×10^{-16}
25/12/2018	29	476	24	22	2.0×10^{-16}
15/01/2019	29	479	25	24	1.5×10^{-16}
25/01/2019	28	506	23	26	1.8×10^{-16}
14/02/2019	36	786	21	29	1.9×10^{-16}

a

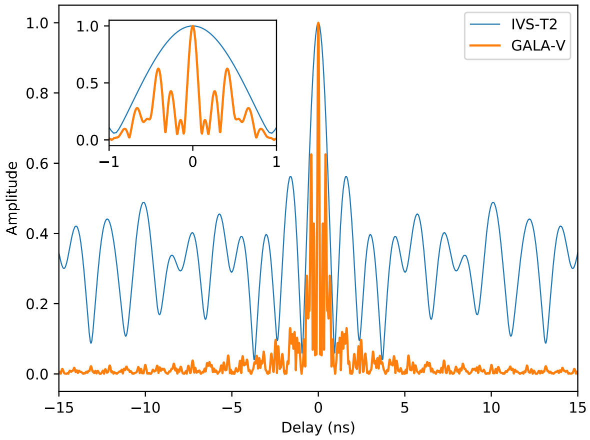

b

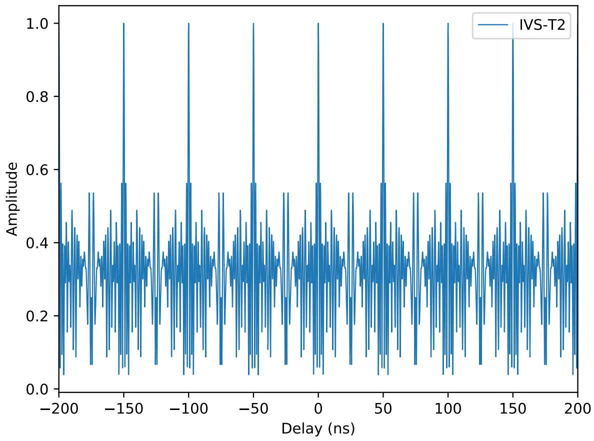

Extended Data Figure 1: Delay resolution function of GALA-V and standard geodetic VLBI (IVS-T2 session). a, Delay resolution functions for the frequency array of GALA-V described in the text and for standard geodetic VLBI (Experiment code T2126). GALA-V delay resolution function shows a single peak and fine delay resolution that allows the derivation of the absolute group delay without ambiguity. **b,** The delay resolution function formed from the frequency array of standard geodetic VLBI shows a delay ambiguity with a period equal to the reciprocal of the greatest common denominator of the frequency interval.

a

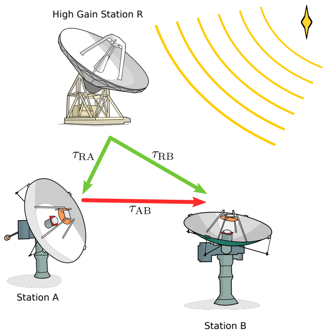

b

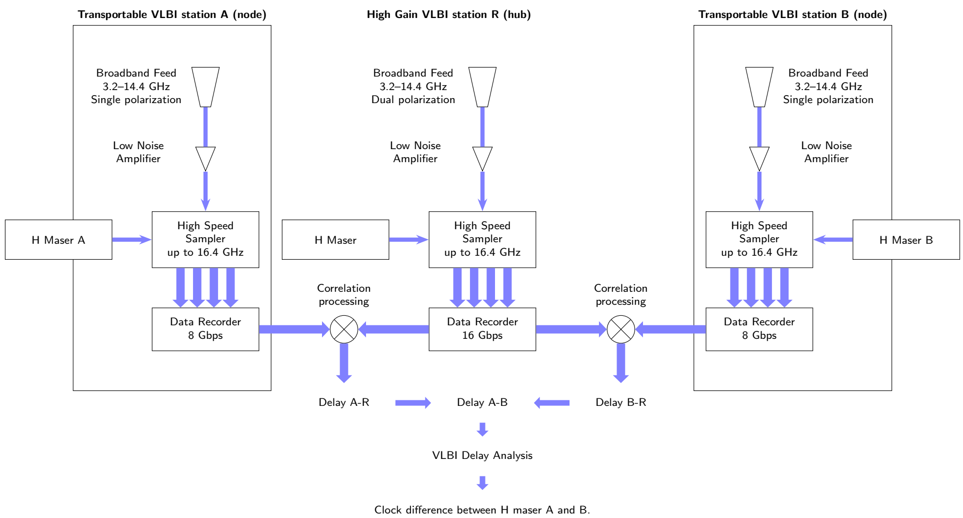

Extended Data Figure 2: Node-hub style observations with transportable broadband VLBI stations. a, Transportable small VLBI stations A and B can be used for intercontinental baseline by using a Node-hub style VLBI scheme with the station R. Delay data of AB baseline is computed by linear combination of delay data on RA and RB baselines. **b,** Block diagram of the Node-hub measurement with the broadband VLBI system.

a

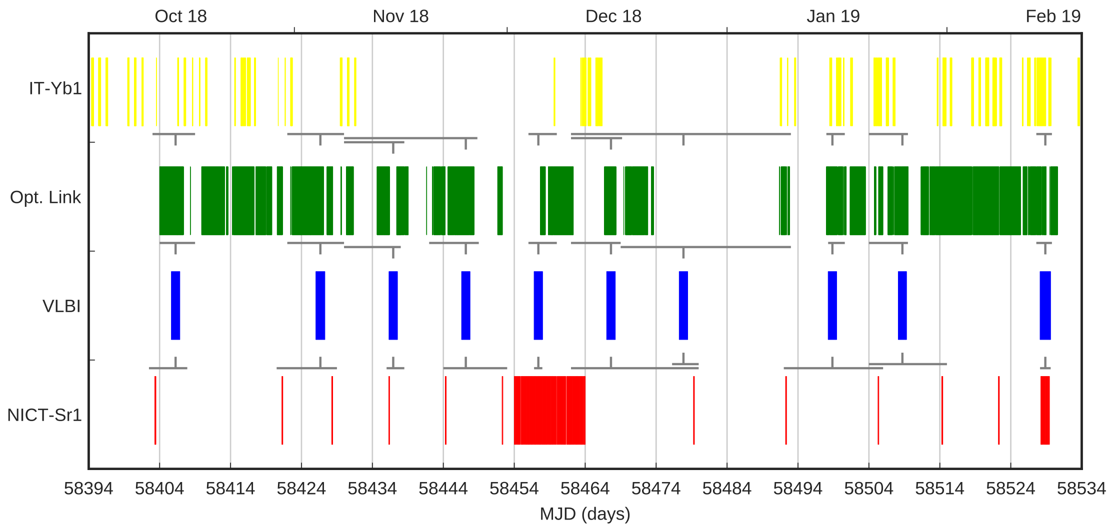

b

Maser	$h_{-2}^{1/2}$	$h_{-1}^{1/2}$	$h_0^{1/2}$	$h_2^{1/2}$
$\mathrm{H_T}$	1.5×10^{-13}	3.5×10^{-14}	5×10^{-16}	2.5×10^{-22}
$\mathrm{H_M}$	1.5×10^{-13}	2.8×10^{-14}	4×10^{-16}	2.5×10^{-22}
$\mathrm{H_K}$	1.1×10^{-13}	4.5×10^{-14}	8×10^{-17}	2.5×10^{-22}

Extended Data Figure 3: Extrapolations over dead times using the masers as a flywheel. a, Uptimes of IT-Yb1 (yellow), optical link (green), VLBI link (blue) and NICT-Sr1 (red) marked as colored regions as a function of MJD. Gray horizontal bars represent evaluation intervals corresponding to each VLBI session, as marked by a vertical notch. For each evaluation interval the extrapolation was calculated for the masers at INRIM (between IT-Yb1 and the optical link), INAF (between the optical link and VLBI), and NICT (between VLBI and NICT-Sr1). **b,** Noise models used for extrapolations for the masers at INRIM, INAF, and NICT, describing the Hadamard variance $\sigma_{\mathrm{H}}^2 = h_{-2}(\tau/\mathrm{s})^{-2} + h_{-1}(\tau/\mathrm{s})^{-1} + h_0 + h_2(\tau/\mathrm{s})^2$.

a

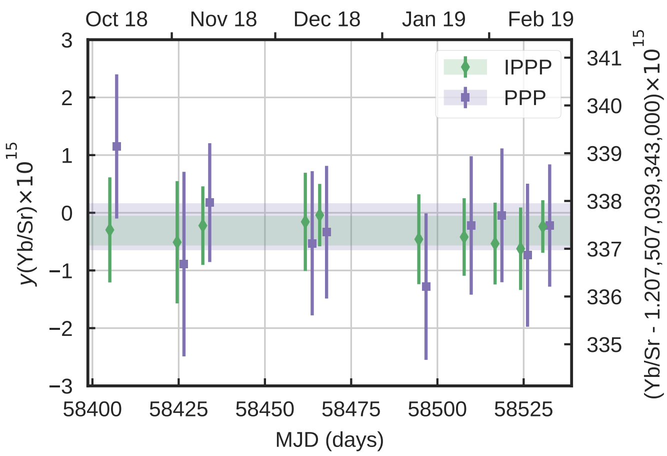

b

Yb/Sr ratio via PPP		Yb/Sr ratio via IPPP	
Contribution	Uncer. ($\times 10^{-16}$)	Contribution	Uncer. ($\times 10^{-16}$)
PPP satellite transfer	3.3	IPPP satellite transfer	1.4
Clocks	0.9	Clocks	0.9
Combs (microwave/optical)	1.1	Combs (microwave/optical)	1.1
Extrapolation	1.8	Extrapolation	1.4
Total	4.0	Total	2.5

Extended Data Figure 4: Yb/Sr frequency ratio measurements between INRIM and NICT measured with a GPS link using IPPP or PPP. a, Plot of the frequency ratio measurements. Green points represent the IPPP comparison with its total uncertainty. Green shaded region is the weighted mean of the IPPP comparison with its total uncertainty. Purple points represent the PPP comparison with its total uncertainty. Purple shaded region is the weighted mean of the PPP comparison with its total uncertainty. Horizontal offset between the two dataset is just for clarity. **b,** Uncertainty budget for the satellite comparisons.

References

[1] McGrew, W. F. *et al.* Atomic clock performance enabling geodesy below the centimetre level. *Nature* **564**, 87–90 (2018). URL https://doi.org/10.1038/s41586-018-0738-2.

[2] Ushijima, I., Takamoto, M., Das, M., Ohkubo, T. & Katori, H. Cryogenic optical lattice clocks. *Nature Photonics* **9**, 185–189 (2015). URL http://dx.doi.org/10.1038/nphoton.2015.5.

[3] Brewer, S. M. *et al.* $^{27}\mathrm{Al}^{+}$ quantum-logic clock with a systematic uncertainty below 10^{-18}. *Physical Review Letters* **123**, 033201 (2019). URL https://link.aps.org/doi/10.1103/PhysRevLett.123.033201.

[4] Wynands, R. & Weyers, S. Atomic fountain clocks. *Metrologia* **42**, S64 (2005). URL http://stacks.iop.org/0026-1394/42/i=3/a=S08.

[5] Panfilo, G. & Arias, F. The coordinated universal time (UTC). *Metrologia* **56**, 042001 (2019). URL https://doi.org/10.1088%2F1681-7575%2Fab1e68.

[6] Riehle, F., Gill, P., Arias, F. & Robertsson, L. The CIPM list of recommended frequency standard values: guidelines and procedures. *Metrologia* **55**, 188 (2018). URL http://stacks.iop.org/0026-1394/55/i=2/a=188.

[7] Sanner, C. *et al.* Optical clock comparison for Lorentz symmetry testing. *Nature* **567**, 204–208 (2019). URL https://doi.org/10.1038/s41586-019-0972-2.

[8] Delva, P. *et al.* Test of special relativity using a fiber network of optical clocks. *Physical Review Letters* **118**, 221102 (2017). URL https://link.aps.org/doi/10.1103/PhysRevLett.118.221102.

[9] Takamoto, M. *et al.* Test of general relativity by a pair of transportable optical lattice clocks. *Nature Photonics* (2020). URL https://doi.org/10.1038/s41566-020-0619-8.

[10] Godun, R. M. *et al.* Frequency Ratio of Two Optical Clock Transitions in $^{171}\mathrm{Yb}^{+}$ and Constraints on the Time Variation of Fundamental Constants. *Physical Review Letters* **113**, 210801 (2014). URL http://link.aps.org/doi/10.1103/PhysRevLett.113.210801.

[11] Huntemann, N. *et al.* Improved Limit on a Temporal Variation of m_p/m_e from Comparisons of Yb^{+} and Cs Atomic Clocks. *Physical Review Letters* **113**, 210802 (2014). URL http://link.aps.org/doi/10.1103/PhysRevLett.113.210802.

[12] Delva, P., Denker, H. & Lion, G. *Relativistic Geodesy*, chap. Chronometric Geodesy: Methods and Applications, 25–85 (Springer International Publishing, Cham, 2019). URL https://doi.org/10.1007/978-3-030-11500-5_2.

[13] Grotti, J. *et al.* Geodesy and metrology with a transportable optical clock. *Nature Physics* **14**, 437–441 (2018). URL https://doi.org/10.1038/s41567-017-0042-3.

[14] Bondarescu, R. *et al.* Ground-based optical atomic clocks as a tool to monitor vertical surface motion. *Geophysical Journal International* **202**, 1770–1774 (2015). URL https://doi.org/10.1093/gji/ggv246. http://oup.prod.sis.lan/gji/article-pdf/202/3/1770/27716716/ggv246.pdf.

[15] Derevianko, A. & Pospelov, M. Hunting for topological dark matter with atomic clocks. *Nature Physics* **10**, 933– (2014). URL https://doi.org/10.1038/nphys3137.

[16] Kómár, P. *et al.* A quantum network of clocks. *Nature Physics* **10**, 582–587 (2014). URL https://doi.org/10.1038/nphys3000.

[17] Kolkowitz, S. *et al.* Gravitational wave detection with optical lattice atomic clocks. *Phys. Rev. D* **94**, 124043 (2016). URL https://link.aps.org/doi/10.1103/PhysRevD.94.124043.

[18] Lisdat, C. *et al.* A clock network for geodesy and fundamental science. *Nature Communications* **7**, 12443– (2016). URL http://dx.doi.org/10.1038/ncomms12443.

[19] Clivati, C. *et al.* Optical frequency transfer over submarine fiber links. *Optica* **5**, 893–901 (2018). URL http://www.osapublishing.org/optica/abstract.cfm?URI=optica-5-8-893.

[20] Hachisu, H. *et al.* Direct comparison of optical lattice clocks with an intercontinental baseline of 9000 km. *Optics Letters* **39**, 4072–4075 (2014). URL http://ol.osa.org/abstract.cfm?URI=ol-39-14-4072.

[21] Riedel, F. *et al.* Direct comparisons of European primary and secondary frequency standards via satellite techniques. *Metrologia* (2020). URL https://doi.org/10.1088/1681-7575/ab6745. Not yet published in print.

[22] Fujieda, M. *et al.* Advanced satellite-based frequency transfer at the 10-16 level. *IEEE Transactions on Ultrasonics, Ferroelectrics, and Frequency Control* **65**, 973–978 (2018).

[23] Leute, J. *et al.* Frequency comparison of $^{171}Yb^{+}$ ion optical clocks at PTB and NPL via GPS PPP. *IEEE Transactions on Ultrasonics, Ferroelectrics, and Frequency Control* **63**, 981–985 (2016).

[24] Event Horizon Telescope Collaboration. First M87 event horizon telescope results. I. the shadow of the supermassive black hole. *Astrophysical Journal Letters* **875** (2019).

[25] Schuh, H. & Behrend, D. VLBI: a fascinating technique for geodesy and astrometry. *Journal of Geodynamics* **61**, 68 – 80 (2012). URL http://www.sciencedirect.com/science/article/pii/S0264370712001159.

[26] Coates, R. J. & Clark, T. A. Worldwide time and frequency synchronization by planned VLBI network. In *Proc. of the Sixth Ann. Precise Time and Time Interval (PTTI) Planning Meeting*, 361–371 (1974).

[27] Clark, T. A. *et al.* Synchronization of clocks by very-long-baseline interferometry. *IEEE Transactions on Instrumentation and Measurement* **28**, 184–187 (1979).

[28] Hobiger, T., Rieck, C., Haas, R. & Koyama, Y. Combining GPS and VLBI for inter-continental frequency transfer. *Metrologia* **52**, 251–261 (2015). URL https://doi.org/10.1088%2F0026-1394%2F52%2F2%2F251.

[29] Koyama, Y. The use of very long baseline interferometry for time and frequency metrology. *MAPAN* **27**, 23–30 (2012). URL https://doi.org/10.1007/s12647-012-0005-1.

[30] Fey, A. L. *et al.* The second realization of the international celestial reference frame by very long baseline interferometry. *The Astronomical Journal* **150**, 58 (2015). URL https://doi.org/10.1088%2F0004-6256%2F150%2F2%2F58.

[31] Boehm, J., Werl, B. & Schuh, H. Troposphere mapping functions for GPS and very long baseline interferometry from European Centre for Medium-Range Weather Forecasts operational analysis data. *Journal of Geophysical Research: Solid Earth* **111** (2006). URL https://agupubs.onlinelibrary.wiley.com/doi/abs/10.1029/2005JB003629. https://agupubs.onlinelibrary.wiley.com/doi/pdf/10.1029/2005JB003629.

[32] Niell, A. *et al.* Demonstration of a broadband very long baseline interferometer system: A new instrument for high-precision space geodesy. *Radio Science* **53**, 1269–1291 (2018). URL https://agupubs.onlinelibrary.wiley.com/doi/abs/10.1029/2018RS006617.

https://agupubs.onlinelibrary.wiley.com/doi/pdf/10.1029/2018RS006617.

[33] Kondo, T. & Takefuji, K. An algorithm of wideband bandwidth synthesis for geodetic VLBI. *Radio Science* **51**, 1686–1702 (2016). URL https://agupubs.onlinelibrary.wiley.com/doi/abs/10.1002/2016RS006070. https://agupubs.onlinelibrary.wiley.com/doi/pdf/10.1002/2016RS006070.

[34] Pizzocaro, M. *et al.* Absolute frequency measurement of the $^1S_0 - {}^3P_0$ transition of ^{171}Yb with a link to international atomic time. *Metrologia* (2019). URL https://doi.org/10.1088/1681-7575/ab50e8. Not yet published in print.

[35] Hachisu, H., Petit, G., Nakagawa, F., Hanado, Y. & Ido, T. SI-traceable measurement of an optical frequency at the low 1×10^{-16} level without a local primary standard. *Optics Express* **25**, 8511–8523 (2017). URL http://www.opticsexpress.org/abstract.cfm?URI=oe-25-8-8511.

[36] Hachisu, H., Nakagawa, F., Hanado, Y. & Ido, T. Months-long real-time generation of a time scale based on an optical clock. *Scientific Reports* **8**, 4243– (2018). URL https://doi.org/10.1038/s41598-018-22423-5.

[37] Recommended values of standard frequencies for applications including the practical realization of the metre and secondary representations of the definition of the second. URL https://www.bipm.org/en/publications/mises-en-pratique/standard-frequencies.html.

[38] Takamoto, M. *et al.* Frequency ratios of Sr, Yb, and Hg based optical lattice clocks and their applications. *Comptes Rendus Physique* **16**, 489 – 498 (2015). URL http://www.sciencedirect.com/science/article/pii/S1631070515000730.

[39] Nemitz, N. *et al.* Frequency ratio of Yb and Sr clocks with 5×10^{-17} uncertainty at 150 seconds averaging time. *Nature Photonics* **10**, 258–261 (2016). URL http://dx.doi.org/10.1038/nphoton.2016.20.

[40] Udem, T., Holzwarth, R. & Hänsch, T. Femtosecond optical frequency combs. *The European Physical Journal Special Topics* **172**, 69–79 (2009). URL https://doi.org/10.1140/epjst/e2009-01042-6.

[41] Clivati, C. *et al.* A VLBI experiment using a remote atomic clock via a coherent fibre link. *Scientific Reports* **7**, 40992– (2017). URL https://doi.org/10.1038/srep40992.

[42] Hachisu, H. & Ido, T. Intermittent optical frequency measurements to reduce the dead time uncertainty of frequency link. *Japanese Journal of Applied Physics* **54**, 112401 (2015). URL http://stacks.iop.org/1347-4065/54/i=11/a=112401.

[43] Grebing, C. *et al.* Realization of a timescale with an accurate optical lattice clock. *Optica* **3**, 563–569 (2016). URL http://www.osapublishing.org/optica/abstract.cfm?URI=optica-3-6-563.

[44] Petit, G. *et al.* 1×10^{-16} frequency transfer by GPS PPP with integer ambiguity resolution. *Metrologia* **52**, 301–309 (2015). URL https://doi.org/10.1088%2F0026-1394%2F52%2F2%2F301.

[45] Johnson, L. A. M., Gill, P. & Margolis, H. S. Evaluating the performance of the NPL femtosecond frequency combs: agreement at the 10-21level. *Metrologia* **52**, 62–71 (2015). URL https://doi.org/10.1088%2F0026-1394%2F52%2F1%2F62.

[46] Xu, M. H. *et al.* Structure effects for 3417 celestial reference frame radio sources. *The Astrophysical Journal Supplement Series* **242**, 5 (2019). URL https://doi.org/10.3847%2F1538-4365%2Fab16ea.

[47] Bolotin, S. *et al.* The source structure effect in broadband observations. In *Proc. of 24th Meeting of the European VLBI Group for Geodesy and Astrometry* (2019).

[48] Riehle, F. Optical clock networks. *Nature Photonics* **11**, 25– (2017). URL https://doi.org/10.1038/nphoton.2016.235.

[49] Fujieda, M. *et al.* Carrier-phase two-way satellite frequency transfer over a very long baseline. *Metrologia* **51**, 253–262 (2014). URL https://doi.org/10.1088%2F0026-1394%2F51%2F3%2F253.

[50] Laurent, P., Massonnet, D., Cacciapuoti, L. & Salomon, C. The ACES/PHARAO space mission. *Comptes Rendus Physique* **16**, 540 – 552 (2015). URL http://www.sciencedirect.com/science/article/pii/S1631070515000808. The measurement of time / La mesure du temps.

[51] Clark, T. A. *et al.* Precision geodesy using the Mark-III very-long-baseline interferometer system. *IEEE Transactions on Geoscience and Remote Sensing* **GE-23**, 438–449 (1985).

[52] Sekido, M. *et al.* An overview of the Japanese GALA-V wideband VLBI system. In Behrend, D., Baver, K. D. & Armstrong, K. L. (eds.) *IVS 2016 General Meeting Proceedings "New Horizons with VGOS"*, NASA/CP-2016-219016, 25–33 (2016).

[53] Ujihara, H., Takefuji, K., Sekido, M. & Ichikawa, R. Development of wideband antennas. In Freymueller, J. T. & Sánchez, L. (eds.) *International Symposium on Advancing Geodesy in a Changing World*, 25–28 (Springer International Publishing, Cham, 2019).

[54] Rogers, A. E. E. Very long baseline interferometry with large effective bandwidth for phase-delay measurements. *Radio Science* **5**, 1239–1247 (1970). URL https://agupubs.onlinelibrary.wiley.com/doi/abs/10.1029/RS005i010p01239. https://agupubs.onlinelibrary.wiley.com/doi/pdf/10.1029/RS005i010p01239.

[55] Takefuji, K. *et al.* High-order sampling techniques of aliased signals for very long baseline interferometry. *Publications of the Astronomical Society of the Pacific* **124**, 1105–1112 (2012). URL https://doi.org/10.1086%2F668232.

[56] Clark, T. A. Geodetic interferometry submission for the IUGG quadrennial report reviews of geophysics and space physics. *Reviews of Geophysics* **17**, 1430–1437 (1979). URL https://agupubs.onlinelibrary.wiley.com/doi/abs/10.1029/RG017i006p01430. https://agupubs.onlinelibrary.wiley.com/doi/pdf/10.1029/RG017i006p01430.

[57] Hase, H., Bäer, A., Riepl, S. & Schlüter, W. Transportable integrated geodetic observatory (tigo). In *International VLBI Service for Geodesy and Astrometry 2000 General Meeting Proceedings*, 383–387 (2000).

[58] Xu, M. H. *et al.* The source structure of 0642+449 detected from the CONT14 observations. *The Astronomical Journal* **152**, 151 (2016). URL https://doi.org/10.3847%2F0004-6256%2F152%2F5%2F151.

[59] Kimura, M. Development of the software correlator for the VERA system III. *IVS NICT-TDC News* **29**, 12–14 (2008).

[60] Gordon, D. *et al.* GSFC VLBI Analysis Center Report. In Baver, K. D., Behrend, D. & Armstrong, K. L. (eds.) *International VLBI Service for Geodesy and Astrometry 2015+2016 Biennial Report*, NASA/TP–2017–219021 (2017). URL http://ivscc.gsfc.nasa.gov/publications/br_2015_2016/index.html.

[61] International Astronomical Union (IAU). Resolution B2 of the thirtieth general assembly of the IAU on the third realization of the international celestial reference frame (2018). URL https://www.iau.org/administration/resolutions/general_assemblies/.

[62] Petit, G. & Luzum, B. IERS conventions (2010). IERS Technical Note 36, International Earth Rotation and Reference Systems Service (IERS), Frankfurt am Main (2010). ISBN 3-89888-989-6.

[63] Saastamoinen, J. *Atmospheric Correction for the Troposphere and Stratosphere in Radio Ranging Satellites*, 247–251 (American Geophysical Union (AGU), 2013). URL https://agupubs.onlinelibrary.wiley.com/doi/abs/10.1029/GM015p0247. https://agupubs.onlinelibrary.wiley.com/doi/pdf/10.1029/GM015p0247.

[64] Landskron, D. & Böhm, J. VMF3/GPT3: refined discrete and empirical troposphere mapping functions. *Journal of Geodesy* **92**, 349–360 (2018). URL https://doi.org/10.1007/s00190-017-1066-2.

[65] Pizzocaro, M. *et al.* Absolute frequency measurement of the $^1S_0 - {}^3P_0$ transition of ^{171}Yb. *Metrologia* **54**, 102 (2017). URL http://stacks.iop.org/0026-1394/54/i=1/a=102.

[66] Takamoto, M., Hong, F.-L., Higashi, R. & Katori, H. An optical lattice clock. *Nature* **435**, 321–324 (2005). URL http://dx.doi.org/10.1038/nature03541.

[67] Sherman, J. A. *et al.* High-accuracy measurement of atomic polarizability in an optical lattice clock. *Physical Review Letters* **108**, 153002 (2012). URL http://link.aps.org/doi/10.1103/PhysRevLett.108.153002.

[68] Beloy, K. *et al.* Atomic clock with 1×10^{-18} room-temperature blackbody stark uncertainty. *Physical Review Letters* **113**, 260801 (2014). URL http://link.aps.org/doi/10.1103/PhysRevLett.113.260801.

[69] Middelmann, T., Falke, S., Lisdat, C. & Sterr, U. High accuracy correction of blackbody radiation shift in an optical lattice clock. *Physical Review Letters* **109**, 263004 (2012). URL http://link.aps.org/doi/10.1103/PhysRevLett.109.263004.

[70] Nemitz, N., Jørgensen, A. A., Yanagimoto, R., Bregolin, F. & Katori, H. Modeling light shifts in optical lattice clocks. *Phys. Rev. A* **99**, 033424 (2019). URL https://link.aps.org/doi/10.1103/PhysRevA.99.033424.

[71] Brown, R. C. *et al.* Hyperpolarizability and operational magic wavelength in an optical lattice clock. *Physical Review Letters* **119**, 253001 (2017). URL https://link.aps.org/doi/10.1103/PhysRevLett.119.253001.

[72] Westergaard, P. G. *et al.* Lattice-induced frequency shifts in Sr optical lattice clocks at the 10^{-17} level. *Physical Review Letters* **106**, 210801 (2011). URL http://link.aps.org/doi/10.1103/PhysRevLett.106.210801.

[73] Ludlow, A. D. *et al.* Sr lattice clock at 1×10^{-16} fractional uncertainty by remote optical evaluation with a Ca clock. *Science* **319**, 1805–1808 (2008). URL http://www.sciencemag.org/content/319/5871/1805.abstract. http://www.sciencemag.org/content/319/5871/1805.full.pdf.

[74] Falke, S. *et al.* The ^{87}Sr optical frequency standard at PTB. *Metrologia* **48**, 399 (2011). URL http://stacks.iop.org/0026-1394/48/i=5/a=022.

[75] Bloom, B. J. *et al.* An optical lattice clock with accuracy and stability at the 10-18 level. *Nature* **506**, 71–75 (2014). URL http://dx.doi.org/10.1038/nature12941.

[76] Nicholson, T. *et al.* Systematic evaluation of an atomic clock at 2×10^{-18} total uncertainty. *Nat Commun* **6**, – (2015). URL http://dx.doi.org/10.1038/ncomms7896.

[77] Gibble, K. Scattering of cold-atom coherences by hot atoms: Frequency shifts from background-gas collisions. *Physical Review Letters* **110**, 180802 (2013). URL http://link.aps.org/doi/10.1103/PhysRevLett.110.180802.

[78] Baillard, X. *et al.* Accuracy evaluation of an optical lattice clock with bosonic atoms. *Optics Letters* **32**, 1812–1814 (2007). URL http://ol.osa.org/abstract.cfm?URI=ol-32-13-1812.

[79] General Conference on Weights and Measures (CGPM). Resolution 2 of its 26th meeting (2018). URL https://www.bipm.org/en/cgpm-2018/.

[80] Margolis, H. *et al.* International timescales with optical clocks (ITOC). In *European Frequency and Time Forum International Frequency Control Symposium (EFTF/IFC), 2013 Joint*, 908–911 (2013).

[81] Denker, H. *et al.* Geodetic methods to determine the relativistic redshift at the level of 10^{-18} in the context of international timescales: a review and practical results. *Journal of Geodesy* **92**, 487–516 (2018). URL https://doi.org/10.1007/s00190-017-1075-1.

[82] Miyahara, B., Kodama, T. & Kuroishi, Y. Development of new hybrid geoid model for Japan, "GSIGEO2011". In *Bulletin of the Geospatial Information Authority of Japan*, vol. 62 (2014).

[83] Clivati, C. *et al.* A coherent fiber link for very long baseline interferometry. *IEEE Transactions on Ultrasonics, Ferroelectrics, and Frequency Control* **62**, 1907–1912 (2015).

[84] Barbieri, P., Clivati, C., Pizzocaro, M., Levi, F. & Calonico, D. Spectral purity transfer with 5×10^{-17} instability at 1 s using a multibranch Er:fiber frequency comb. *Metrologia* (2019). URL http://iopscience.iop.org/10.1088/1681-7575/ab2b0f.

[85] Baynham, C. F. A. *et al.* Absolute frequency measurement of the optical clock transition in with an uncertainty of using a frequency link to international atomic time. *Journal of Modern Optics* **65**, 585–591 (2017). URL https://doi.org/10.1080/09500340.2017.1384514. https://doi.org/10.1080/09500340.2017.1384514.

[86] Yu, D.-H., Weiss, M. & Parker, T. E. Uncertainty of a frequency comparison with distributed dead time and measurement interval offset. *Metrologia* **44**, 91 (2007). URL http://stacks.iop.org/0026-1394/44/i=1/a=014.

[87] Riley, W. J. Handbook of frequency stability analysis. NIST Special Publication 1065, National Institute of Standards and Technology (2008).

[88] Kasdin, N. J. & Walter, T. Discrete simulation of power law noise (for oscillator stability evaluation). In *Proceedings of the 1992 IEEE Frequency Control Symposium*, 274–283 (1992).

[89] Nakagawa, F., Imae, M., Hanado, Y. & Aida, M. Development of multichannel dual-mixer time difference system to generate UTC(NICT). *IEEE Transactions on Instrumentation and Measurement* **54**, 829–832 (2005).

[90] Luenberger, D. G. *Optimization by Vector Space Methods* (Wiley, New York, 1998).

[91] Margolis, H. S. & Gill, P. Least-squares analysis of clock frequency comparison data to deduce optimized frequency and frequency ratio values. *Metrologia* **52**, 628 (2015). URL http://stacks.iop.org/0026-1394/52/i=5/a=628.